Depletion interactions in colloid-polymer mixtures

X. Ye, T. Narayanan, and P. Tong*
Department of Physics, Oklahoma State University, Stillwater, Oklahoma 74078

J. S. Huang and M. Y. Lin
Exxon Research and Engineering Company, Route 22 East, Annandale, New Jersey 08801

B. L. Carvalho
Department of Materials Science and Engineering, Massachusetts Institute of Technology, Cambridge, Massachusetts 02139

L. J. Fetters
Exxon Research and Engineering Company, Route 22 East, Annandale, New Jersey 08801
(Received 10 May 1996)

We present a neutron-scattering study of depletion interactions in a mixture of a hard-sphere-like colloid and a nonadsorbing polymer. By matching the scattering length density of the solvent with that of the polymer, we measured the partial structure factor $S_c(Q)$ for the colloidal particles. It is found that the measured $S_c(Q)$ for different colloid and polymer concentrations can be well described by an effective interaction potential $U(r)$ for the polymer-induced depletion attraction between the colloidal particles. The magnitude of the attraction is found to increase linearly with the polymer concentration, but it levels off at higher polymer concentrations. This reduction in the depletion attraction presumably arises from the polymer-polymer interactions. The experiment demonstrates the effectiveness of using a nonadsorbing polymer to control the magnitude as well as the range of the interaction between the colloidal particles. [S1063-651X(96)10911-9]

PACS number(s): 82.70.Dd, 61.12.Ex, 65.50.+m, 61.25.Hq

I. INTRODUCTION

Microscopic interactions between colloidal particles in polymer solutions control the phase stability of many colloid-polymer mixtures, which are directly of interest to industries. Lubricating oils and paint are examples of the colloid-polymer mixtures in which phase stability is desired. The interaction between the colloidal particles can be expressed in terms of an effective potential $U(r)$, which is the work required to bring two colloidal particles from infinity to a distance r in a given polymer solution [1]. In the study of the interactions in colloid-polymer mixtures, it is important to distinguish between polymers that are adsorbed on the colloidal surfaces and those that are free in solutions, because the two situations usually lead to qualitatively different effects. In a mixture of a colloid and a nonadsorbing polymer, the potential $U(r)$ can develop an attractive well because of the depletion effect [1,2] in that the polymer chains are expelled from the region between two colloidal particles when their surface separation becomes smaller than the size of the polymer chains. The exclusion of polymer molecules from the space between the colloidal particles leads to an unbalanced osmotic pressure difference pushing the colloidal particles together, which results in an effective attraction between the two colloidal particles. If the attraction is large enough, phase separation occurs in the colloid-polymer mixture [3,4]. In the case of adsorption, the adsorbed polymer chains, in a good solvent, resist the approach of other surfaces through a loss of conformational entropy. Colloidal surfaces are then maintained at separations large enough to damp any attractions due to the depletion effect or London–van der Waals force and the colloidal suspension is stabilized [5,6].

In addition to its important practical applications, the study of the colloid-polymer mixtures is also of fundamental interest in statistical mechanics. The recent theoretical calculations [7–10] for the entropy-driven phase separation in binary mixtures of hard spheres have stimulated considerable experimental efforts to study the phase behavior of various binary mixtures, such as liquid emulsions [11], binary colloidal mixtures [12–15], colloid-surfactant mixtures [16], binary emulsions [17], and mixtures of colloids with nonadsorbing polymers [18]. While it is successful in explaining the phase behavior of these mixtures, the binary hard-sphere model is nevertheless a highly idealized theoretical model. In reality, there are many complicated, non-hard-sphere colloidal mixtures. Even in the study of the model colloidal mixtures, the particles used in the experiments are stabilized either by surface charges or by a layer of surfactant molecules and hence the interparticle potential has a weak repulsive tail. The interaction potentials for the surfactant aggregates and polymer molecules are probably much softer than that of the hard spheres. Measurements of phase behavior and other thermodynamic properties are useful in studies of macroscopic properties of the binary mixtures, but they are much less sensitive to the details of the molecular interactions in the system. Microscopic measurements, such as radiation-scattering experiments, therefore are needed to directly probe the molecular interactions in the mixtures. With this knowledge, one can estimate the phase stability properties of the-

*Author to whom correspondence should be addressed.

binary mixtures in a straightforward way. (The reverse process of inferring the intermolecular interactions from the phase behavior is much more problematic and unsure.) The study of microscopic interactions complements the macroscopic phase measurements. With both microscopic and macroscopic measurements, one can verify assumptions and test predictions of various theoretical models for the depletion effect [3,4,19,20]. These measurements are also useful for the further development of the depletion theory to a more general form, so that non-hard-sphere interactions can be included.

In contrast to many previous experimental studies [19–22], which mainly focus on the phase behavior of the colloid-polymer mixtures, we have recently carried out a laser light-scattering study of the depletion interaction in a mixture of a hard-sphere-like colloid and a nonadsorbing polymer [23]. In the experiment, the second virial coefficient of the colloidal particles as a function of the free-polymer concentration was obtained from the measured concentration dependence of the scattered light intensity from the mixture. The experiment demonstrated that our light-scattering method is indeed capable of measuring the depletion effect in the colloid-polymer mixture. However, the interpretation of the measurements was somewhat complicated by the unwanted scattering from the polymer. Assumptions were made in order to deal with the interference effect between the colloid and the polymer.

In this paper we report a small-angle neutron scattering (SANS) study of the depletion interaction in the same colloid-polymer mixture. The use of SANS with isotopically mixed solvents eliminates the undesirable scattering from the polymer. In the experiment, we measure the colloidal (partial) structure factor $S_c(Q)$ over a suitable range of the scattering wave number Q. The measured $S_c(Q)$ is directly related to the interaction potential $U(r)$ and therefore it provides more detailed information about the colloidal interaction in the polymer solution than the second virial coefficient does. The colloidal particle chosen for the study consisted of a calcium carbonate ($CaCO_3$) core with an adsorbed monolayer of a randomly branched calcium alkylbenzene sulphonate surfactant. The polymer we used was hydrogenated polyisoprene, a stable straight-chain polymer. Both the polymer and the colloidal particles were dispersed in a good solvent, decane. Such a nonaqueous colloid-polymer mixture is ideal for the investigation attempted here since the colloidal suspension is approximately a hard-sphere system and both the colloid and the polymer have been well characterized previously using various experimental techniques. Because the basic molecular interactions are tuned to be simple, the SANS measurements in the colloid-polymer mixture can be used to critically examine the current theory for the depletion effect [3,4,19,20].

The paper is organized as follows. In Sec. II, we review the scattering theory for a mixture of a colloid and a nonadsorbing polymer and present the calculation of the colloidal structure factor $S_c(Q)$ using the potential $U(r)$ for the polymer-induced depletion attraction. Experimental details appear in Sec. III, and the results are discussed in Sec. IV. Finally, the work is summarized in Sec. V.

II. THEORY

A. Scattering from a mixture of colloidal particles and polymer molecules

Consider the scattering medium to be made of a mixture of colloidal particles and nonadsorbing polymer molecules. The total scattered intensity from the mixture can be written as [23,24]

$$I(Q)=K_c^2\Sigma_{cc}(Q)+2(K_cK_p)\Sigma_{cp}(Q)+K_p^2\Sigma_{pp}(Q), \quad (1)$$

where the subscripts c and p are used, respectively, to identify the colloid and polymer and K_α is the scattering length density of the α component, which has taken into account the contrast between the α component and the solvent. The scattering wave number $Q=(4\pi/\lambda_0)\sin(\theta/2)$, with λ_0 being the wavelength and θ the scattering angle. The function $\Sigma_{\alpha\beta}(Q)$ in Eq. (1) has the form

$$\Sigma_{\alpha\beta}(Q)=\sum_j^{N_\alpha}\sum_l^{N_\beta}\langle e^{-i\mathbf{Q}\cdot(\mathbf{r}_j^\alpha-\mathbf{r}_l^\beta)}\rangle, \quad (2)$$

where r_j^α is the position of the jth monomer of the α component and N_α is the total number of the monomers in the sample volume V. The angular brackets indicate an average over all possible configurations of the molecules.

The function $\Sigma_{\alpha\beta}(Q)$ measures the interaction between the components α and β in the mixture. In the experiment to be described below, we are interested in the polymer-induced depletion attraction between the colloidal particles and thus the scattering length density of the solvent is chosen to be the same as that of the polymer. In this case, the polymer molecules become invisible to neutrons ($K_p=0$) and Eq. (1) becomes

$$I(Q)=K_c^2\rho_cP_c(Q)S_c(Q). \quad (3)$$

In the above, ρ_c is the number density of the colloidal particles and $P_c(Q)$ is their scattering form factor. The partial structure factor $S_c(Q)$ measures the interaction between the colloidal particles and it is proportional to the Fourier transform of the radial distribution function $g_c(r)$ for the colloidal particles. Experimentally, $S_c(Q)$ is obtained by

$$S_c(Q)=\frac{I(Q)}{K_c^2\rho_cP_c(Q)}, \quad (4)$$

where $K_c^2P_c(Q)$ is the scattered intensity per unit concentration measured in a dilute pure colloidal suspension, in which the colloidal interaction is negligible and thus $S_c(Q)=1$.

B. Calculation of the form and structure factors for colloidal particles

As mentioned in Sec. I, our colloidal particle consists of a calcium carbonate core with an adsorbed monolayer of surfactant molecules. A simple core-shell model, as shown in

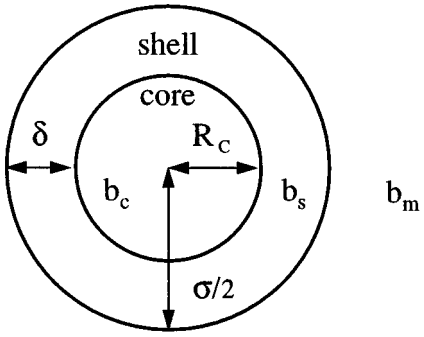

FIG. 1. Simple core-shell model for a colloidal particle consisting of a $CaCO_3$ core with an adsorbed monolayer of surfactant molecules. Here R_c is the core radius, δ is the shell thickness, and b_c, b_s, and b_m are the coherent scattering length densities of the core, shell, and solvent, respectively.

Fig. 1, has been used to characterize the microstructure of the particles [25–27]. The form factor $P_c(Q)$ for the core-shell model is

$$P_c(QR_c)=\left\{(b_c-b_s)\,\frac{4\pi R_c^3}{3}\,f(QR_c)+(b_s-b_m)\,\frac{4\pi(R_c+\delta)^3}{3}\,f[Q(R_c+\delta)]\right\}^2, \quad (5)$$

with

$$f(x)=\frac{3(\sin x - x\,\cos x)}{x^3}. \quad (6)$$

In the above, R_c is the core radius, δ is the shell thickness, and b_c, b_s, and b_m are the coherent scattering length densities of the core, shell, and solvent, respectively.

When the particles are not uniform in size, the average form factor takes the form

$$\langle P_c(Q)\rangle=\int_0^\infty P(QR_c)g(R_c)dR_c, \quad (7)$$

where $g(R_c)$ is the probability distribution for the core radius R_c. To reduce the fitting parameters, we have assumed in Eq. (7) that the shell thickness δ is a constant. Previous experiments [28,29] have shown that for a narrow size distribution $g(R_c)$, the measured $\langle P_c(Q)\rangle$ is not very sensitive to the detail functional form of $g(R_c)$. For simplicity, we now use the Schultz distribution to model the size distribution of our particles. The Schultz distribution function has the form

$$g(R_c)=\frac{(z+1)^{z+1}}{R_0\Gamma(z+1)}\left(\frac{R_c}{R_0}\right)^z e^{-(z+1)R_c/R_0}, \quad (8)$$

where R_0 is the mean core radius and $\Gamma(x)$ is the gamma function. The normalized standard deviation (or the polydispersity) ϵ is related to the parameter z via $\epsilon\equiv\langle(R_c-R_0)^2\rangle^{1/2}/R_0=(z+1)^{-1/2}$. With the Schultz distribution function, one can calculate $\langle P_c(Q)\rangle$ in Eq. (7) using a simple numerical integration method.

To calculate the structure factor $S_c(Q)$, one needs first to solve the Ornstein-Zernike equation for the direct correlation function $C(r)$ using a known interaction potential $U(r)$ [30]. Asakura and Oosawa [1] have derived an effective interaction potential $U(r)$ for the colloidal particles in a nonadsorbing polymer solution. It is assumed in the model that the colloidal particles are hard spheres and the polymer molecules behave as hard spheres toward the colloidal particles but can freely penetrate with each other. Under this approximation, $U(r)$ takes the form [1,2]

$$U(r)=\begin{cases}+\infty, & r\leqslant\sigma\\ -\Pi_p V_0(r), & \sigma<r\leqslant\sigma+2R_g\\ 0, & r>\sigma+2R_g,\end{cases} \quad (9)$$

where σ is the particle diameter, Π_p is the osmotic pressure of the polymer molecules, and R_g is their radius of gyration. The volume of the overlapping depletion zones between the two colloidal particles at a separation r is given by [1,2]

$$V_0(r)=v_p\left(\frac{\lambda}{\lambda-1}\right)^3\left[1-\frac{3}{2}\left(\frac{r}{\sigma\lambda}\right)+\frac{1}{2}\left(\frac{r}{\sigma\lambda}\right)^3\right], \quad (10)$$

where $v_p=(4\pi/3)R_g^3$ is the volume occupied by a polymer chain and $\lambda=1+2R_g/\sigma$. This potential has been used to calculate the phase diagram of the binary system [3,4], and recent phase measurements of several colloid-polymer mixtures have shown qualitative agreement with the calculation [18–20].

When the potential $U(r)$ is constituted by a hard core plus a weak attractive tail as in Eq. (9), the direct correlation function $C(r)$ can be obtained under the mean spherical approximation (MSA), which is a perturbative treatment to the Percus-Yevick equation [30]. Under the MSA, we have

$$C(r)=\begin{cases}C_{\rm HS}(r), & r\leqslant\sigma\\ -U(r)/k_BT, & r>\sigma,\end{cases} \quad (11)$$

where k_BT is the thermal energy and $C_{\rm HS}(r)$ is a known direct correlation function for the simple hard-sphere system [31,32]. Note that $C(r)$ is constituted by two parts: (i) a hard core that involves the colloid diameter σ and its volume fraction ϕ_c and (ii) an attractive tail with the dimensionless amplitude $\tilde{P}=\Pi_p v_p/(k_BT)$ and the range parameter λ. With Eqs. (9)–(11), we calculate the Fourier transform $\tilde{C}(Q)$ of $C(r)$ (see the Appendix) and obtain the structure factor $S_c(Q)$ via the well-known relation [30]

$$S_c(Q)=\frac{1}{1-\rho_c\tilde{C}(Q)}. \quad (12)$$

C. Scattering from flexible polymer chains

Because of the chain flexibility and interchain penetration, the scattered intensity $I(Q)$ from a polymer solution cannot be generally written as a product of the form factor $P_p(Q)$ and the structure factor $S_p(Q)$. However, Zimm has shown [33,34] that when two different polymer chains are assumed to have only a single contact, $P_p(Q)$ can still be factored out from the measured $I(Q)$. Under this single-contact approximation, $I(Q)$ takes the form

$$I(Q)=\frac{K_0\rho_p' M_p P_p(Q)}{1+2(A_2)_p M_p \rho_p' P_p(Q)}. \quad (13)$$

In the above, K_0 is an instrumental constant, ρ_p' is the polymer concentration in g/cm^3, M_p is the molecular weight, and $(A_2)_p$ is the second virial coefficient. Zimm initially derived Eq. (13) in a low polymer concentration limit and later Benoit and Benmouna [35,36] generalized the equation to a high concentration regime using the mean-field theory of Ornstein and Zernike [35]. For a dilute polymer solution, Eq. (13) can be rearranged to read

$$\frac{K_0\rho_p' M_p}{I(Q)}=\frac{1}{P(Q)}+2(A_2)_p M_p \rho_p'. \quad (14)$$

For small values of Q, we have $P_p(Q)\simeq 1-(QR_g)^2/3$ and thus Eq. (14) becomes

$$\frac{K_0\rho_p' M_p}{I(Q)}=1+\frac{1}{3}(QR_g)^2+2(A_2)_p M_p \rho_p'. \quad (15)$$

With Eq. (15) one can obtain values of $K_0 M_p$, R_g^2, and $(A_2)_p M_p$ by linearly extrapolating the scattering data $\rho_p'/I(Q)$ to the limits of $\rho_p'\to 0$ and $Q^2\to 0$, respectively. Using Eq. (13), one can also obtain the polymer structure factor $S_p(Q)=I(Q)/[K_0\rho_p' M_p P_p(Q)]$, which has the form

$$S_p(Q)=\frac{1}{1+2A_2 M_p \rho_p' P_p(Q)}. \quad (16)$$

III. EXPERIMENT

A. Sample preparation

As mentioned in Sec. I, our colloidal particle consists of a $CaCO_3$ core with an adsorbed monolayer of a randomly branched calcium alkylbenzene sulphonate surfactant. The synthesis procedures used to prepare the colloid have been described by Markovic *et al.* [25]. These particles have been well characterized previously using SANS and small-angle x-ray scattering (SAXS) techniques [25–27] and they are used as an acid-neutralizing aid in lubricating oils. The molecular weight of the particle is $M_c=300\,000\pm 15\%$, which was obtained from a sedimentation measurement [23]. The colloidal suspensions were prepared by diluting known amounts of the concentrated suspension with the solvent, decane. The suspensions were then centrifuged at an acceleration of 10^8 cm/s^2 (10^5 g) for 2.5 h to remove any colloidal aggregates and dust. The resulting colloidal suspensions were found to be relatively monodispersed with $\sim$10% standard deviation in the particle radius, as determined by dynamic light scattering [23].

The polymer used in the study was hydrogenated polyisoprene [poly-ethylene-propylene (PEP)], a straight-chain polymer synthesized by an anionic polymerization scheme [37,38]. The PEP is a model polymer (with $M_w/M_n<1.1$), which has been well characterized previously using various experimental techniques [37–39]. The molecular weight of the PEP was $M_p=26\,000$ amu. The molecular weight characterization was carried out by size exclusion chromatography, which was made with a Waters 150-C SEC instrument using μ-Styragel columns and tetrahydrofuran as the elution solvent. To vary the scattering contrast, both hydrogenated decane (Aldrich, >99% pure) and deuterated decane (Cambridge Isotope Laboratories, >99% deuterated) were used as solvents. Decane has been found to be a good solvent for both the colloid and PEP [23]. The scattering length densities of the colloid, the PEP polymer, and the solvents used in the experiment are listed in Table I. Some of the values in the table are taken from Refs. [25–27].

TABLE I. Scattering length densities of the colloid, polymer, and solvents.

Material	Mass density (g/cm^3)	Scattering length density (10^{10} cm^{-2}) x ray	neutron
$CaCO_3$ core	2	16.8	3.48
surfactant shell	0.9–1.0	8.0–9.5	0.35
PEP polymer	0.856	~6.78	−0.31
decane	0.73	~6.78	−0.49
decane-d_{22}	0.84	~6.78	6.58

B. Small-angle neutron- and x-ray-scattering measurements

The SANS measurements of the pure colloidal samples and the mixture samples were performed at the High Flux Beam Reactor in the Brookhaven National Laboratory. The incident neutron wavelength $\lambda_0=7.05\pm 0.4$ Å and the usable Q range was 0.007 Å$^{-1}\leq Q\leq 0.15$ Å^{-1}. The SANS measurements of the pure polymer samples were performed on a SANS instrument (NG-7) at the National Institute of Standards and Technology. The incident neutron wavelength $\lambda_0=5.00\pm 0.35$ Å and the usable Q range was 0.01 Å$^{-1}\leq Q\leq 0.142$ Å^{-1}. The SAXS measurements of dilute colloidal samples were performed on a high-resolution spectrometer at the Oak Ridge National Laboratory. The incident x-ray wavelength $\lambda_0=1.54\pm 0.04$ Å and the usable Q range was 0.014 Å$^{-1}\leq Q\leq 0.31$ Å^{-1}. All the scattering measurements were conducted at room temperature. The neutron-scattering sample cells were made of quartz and the x-ray-scattering cells were made of Kapton; both types of cells had a path length of 1 mm. The raw scattered intensity $I_r(Q)$ (counts/h) was measured by a two-dimensional detector. The corrected intensity $I(Q)$ was obtained by applying the standard corrections due to the background intensity, solvent scattering and sample turbility via

$$I(Q)=\frac{I_r(Q)-I_b(Q)}{T_r}-\frac{I_s(Q)-I_b(Q)}{T_s} \quad (17)$$

and subsequently computing the azimuthal average. In the above, $I_b(Q)$ is the background scattering when the neutron beam is blocked, $I_s(Q)$ is the scattered intensity from the solvent, and T_r and T_s are the transmission coefficients for the scattering sample and the solvent, respectively. To eliminate the inhomogeneity of detector's sensitivity at different pixels, we normalized the scattering data (both neutron and x-ray) with isotropic scattering standards. The structure factor $S_c(Q)$ for the pure colloid samples and the mixture samples were obtained by using Eq. (4).

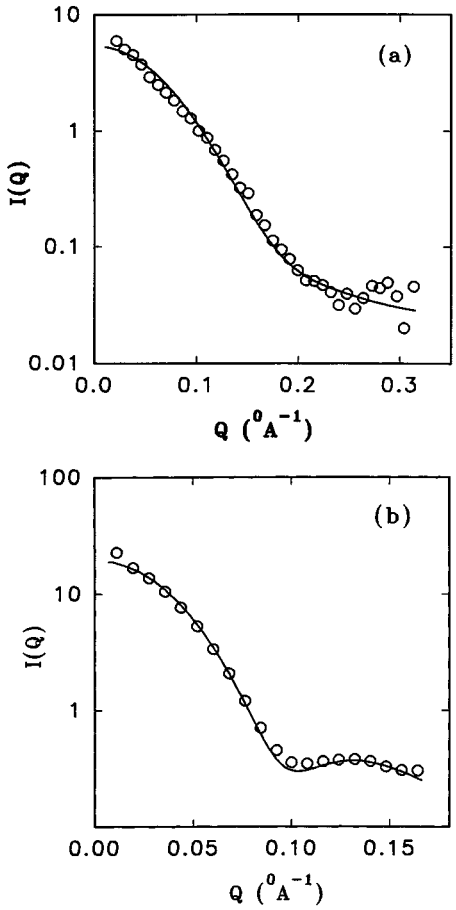

FIG. 2. Measured scattering intensity $I(Q)$ as a function of Q for the dilute pure colloidal suspensions. (a) SAXS data from the colloid-decane suspension at the concentration $\rho_c'=1$ wt. % and (b) SANS data from the colloid–deuterated-decane suspension at $\rho_c'=1$ wt. %. The solid curve in (a) is a fit to the form factor of the polydispersed spheres and that in (b) is a fit to the form factor of the polydispersed core-shell particles.

IV. RESULTS AND DISCUSSION

A. Pure colloids

Figure 2(a) shows the SAXS data for the dilute pure colloidal suspension in decane at the concentration $\rho_c'=1$ wt. %. Because the x-ray-scattering length density for the surfactant shell is about the same as that of decane (see Table I), the scattering is dominated by the $CaCO_3$ core [27]. The solid curve in Fig. 2(a) is the calculated $\langle P_c(Q)\rangle$ for the polydispersed spheres using Eqs. (7), (5), and (8) with $b_s=b_m$. Since the shell thickness δ is absent from the fitting, one can determine the core radius more accurately from the SAXS data. There are three fitting parameters in the plot: the mean core radius R_0, the polydispersity parameter z, and the scattered intensity I_0 at $Q\rightarrow 0$. Figure 2(b) shows the SANS data for the dilute colloidal suspension in deuterated decane at $\rho_c'=1$ wt. %. Because the neutron-scattering length density of the surfactant shell is much different from that of deuterated decane (see Table I), the scattering from the surfactant shell is more pronounced in the SANS data. It is seen from Fig. 2(b) that the scattering from the surfactant shell exhibits a sharp minimum, which entails a tight fit for the shell thickness δ. The solid curve in Fig. 2(b) is the calculated $\langle P_c(Q)\rangle$ for the polydispersed core-shell particles using Eqs. (7), (5), and (8). In the calculation, the neutron-scattering densities for the $CaCO_3$ core, the surfactant shell, and deuterated decane are taken from Table I and R_0 is fixed at the value determined from the SAXS data. As a result, there are only three parameters left in the fitting: δ, z, and I_0. The fitting results for the dilute colloidal suspension are listed in Table II and they agree well with previous SAXS and SANS measurements [25–27]. From the fitted value of z, we find the polydispersity of the core radius to be $\epsilon\simeq 25\%$, which is slightly larger than that determined by dynamic light scattering ($\epsilon\simeq 10\%$) [23]. The fact that the value of z obtained from the SANS data is smaller than that from the SAXS data suggests that the surfactant shell is also somewhat polydispersed [27].

TABLE II. Fitting results from dilute colloid and polymer samples.

Samples	R_0 (nm)	δ (nm)	z	R_g (nm)	R_T (nm)
Colloid-decane (SAXS)	2.0		15.1		
Colloid–decane-d_{22} (SANS)	2.0	2.0	12.0		
PEP–decane-d_{22} (SANS)				8.28	4.85

We now discuss the structure factor $S_c(Q)$ of the concentrated pure colloidal suspensions in decane measured by SANS. Figure 3 shows the measured $S_c(Q)$ for three colloid concentrations: (a) $\rho_c'=26.2$ wt. %, (b) 17.5 wt. %, and (c) 8.7 wt. %. The solid curves are the fits to the simple hard-sphere structure factor [40,41], which can be obtained by taking $U(r)=0$ for $r>\sigma$ in Eq. (11). There are two fitting parameters in the hard-sphere model: the volume fraction ϕ_c and the hard-sphere diameter σ. The fitted values of ϕ_c and σ for different colloidal concentrations are given in Table III. Because the centrifugation process removed some colloidal aggregates and dust from the master colloidal solution, the nominal mass concentration of the colloidal samples has some uncertainties. However, the ratios of the concentrations are accurate and the ratios of the fitted ϕ_c in Table III agree well with them. It is seen from Table III that the fitted σ remains constant for different colloid concentrations and its best fit value is $\sigma=7.7$ nm. This value is very close to the measured particle size $2(R_0+\delta)$ ($=8.0$ nm) as listed in Table II. Because the surfactant shell of the colloidal particle is ''soft,'' we expect its effective hard-shell thickness to be smaller than δ.

Figure 3 clearly shows that the hard-sphere model fits the low concentration data well. As the colloid concentration increases, the measured $S_c(Q)$ starts to deviate from the hard-sphere model in the small-Q region. The deviation can be attributed to a weak repulsion between the soft surfactant shells, since the measured $S_c(0)$ is smaller than the hard-sphere value. The colloidal particles ''feel'' more and more repulsion when their separation is decreased. Because the deviation in the small-Q region is small, the measured $S_c(Q)$ becomes insensitive to the detail functional form of the soft repulsion in $U(r)$. We have tested several functional forms for the repulsive tail, such as an exponential decaying func-

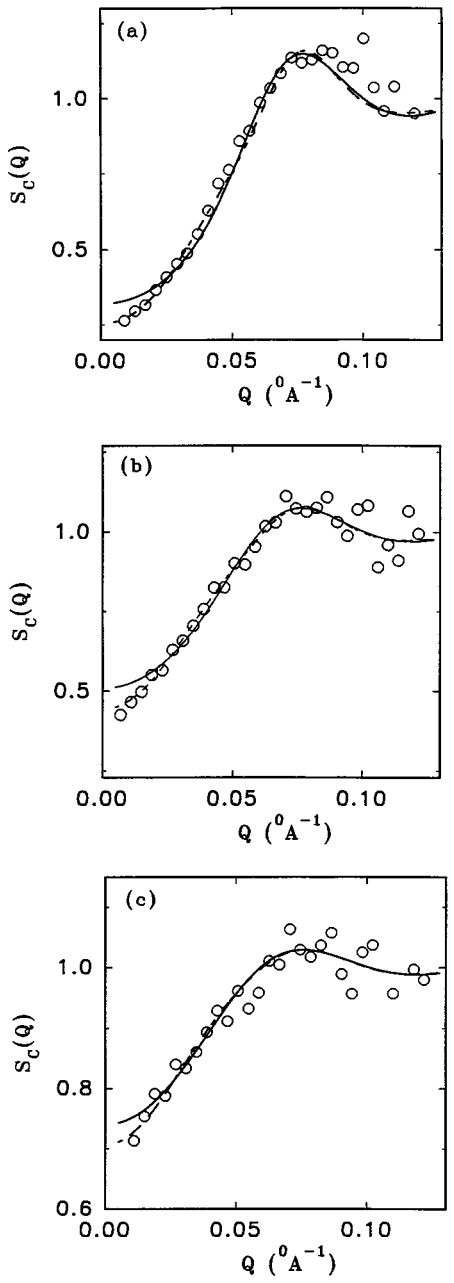

FIG. 3. Measured structure factor $S_c(Q)$ of the concentrated colloid-decane suspensions for three concentrations: (a) $\rho_c'=26.2$ wt. %, (b) 17.5 wt. %, and (c) 8.7 wt. %. The solid curves are the fits to the hard-sphere model and the dashed curves correspond to a hard-core potential with a repulsive barrier.

tion and a square barrier, and found that all these functions fit the data equally well. The dashed curves in Fig. 3 show the calculated $S_c(Q)$ for the hard spheres with a square repulsive barrier, which fit the data better than the hard-sphere model in the small-Q region. Sharma and Sharma [42] have calculated $S_c(Q)$ for a hard-core potential with an attractive square well. Here we simply change the sign of the attractive well to model the repulsive barrier.

There are four parameters in the model: the volume fraction ϕ_c, the diameter σ, the barrier height η (in units of k_BT), and the barrier width γ. A dimensionless parameter λ is defined as $\lambda=1+\gamma/\sigma$. The fitting results are summarized in Table III. It is seen that the fitted values of σ and ϕ_c are the same as those from the hard-sphere model. The fitted barrier height η is found to be small compared to the thermal energy k_BT (the negative sign indicates repulsion) and it increases slightly with the colloid concentration as discussed above. It is also found from the fitting that a fixed value of λ ($=2.0$) can be used to fit all the data with different concentrations. This value of λ suggests that the soft repulsion range is approximately the same as the hard-core diameter σ. Previous SANS measurements for the same colloid have also shown this relatively large interaction range [26]. The above measurements for the pure colloidal samples reveal that the microstructure of the particles can be well described by the simple core-shell model and the colloidal suspension is approximately a hard-sphere system. Our data analysis for the particle form factor is somewhat complicated by the small polydispersity of the samples and the interparticle potential is slightly affected by the weak repulsion between the soft surfactant layers.

TABLE III. Fitting results from concentrated colloid samples.

Colloidal samples (wt. %)	Hard sphere		Hard core plus a square barrier			
	ϕ_c	σ (nm)	ϕ_c	σ (nm)	$\eta\,(k_BT)$	λ
26.2	0.146	7.8	0.146	7.8	−0.1	2.0
17.5	0.086	7.7	0.086	7.7	−0.06	2.0
8.7	0.038	7.7	0.038	7.7	−0.03	2.0

B. Pure polymers

Figure 4(a) shows the Zimm plot of the SANS data for the pure PEP in deuterated decane with the polymer concentration ρ_p' ranging from 0.0072 to 0.0634 g/cm^3. The SANS data are found to be well described by the Zimm relation as shown in Eq. (15) [for clarity we did not draw the linear extrapolation lines in Fig. 4(a)]. From the Zimm analysis, we find that the polymer chains have a radius of gyration $R_g=8.28$ nm and their second virial coefficient $A_2M_p=44.4$ cm^3/g. With the measured A_2 one can define a thermodynamic radius (an effective hard-sphere radius) R_T via $4(4\pi/3)R_T^3=A_2M_p^2$. Thus we have $R_T=4.85$ nm, which agrees well with our previous light-scattering measurement [23]. It is shown in Eq. (14) that when the scattering data $\rho_p'/I(Q)$ at a fixed Q is plotted as a function of ρ_p', a linear extrapolation to $\rho_p'\rightarrow 0$ gives $[K_0M_pP_p(Q)]^{-1}$. The zeroth curve in Fig. 4(a) shows the extrapolated $[K_0M_pP_p(Q)]^{-1}$. Using the known value of K_0M_p ($=0.0036$, determined from the Zimm plot), we obtain the polymer form factor $P_p(Q)$ as shown in Fig. 4(b). The large-Q portion of $P_p(Q)$ is found to be well described by the power law $1/[0.64(QR_g)^{1/\nu}]$ (solid line), with $\nu=\frac{3}{5}$ being the Flory exponent for three-dimensional polymer chains [43].

With the extrapolated $P_p(Q)$, one can obtain the polymer structure factor $S_p(Q)=I(Q)/[K_0\rho_p'M_pP_p(Q)]$ from the concentrated polymer samples. Figure 5 shows the measured $S_p(Q)$ of the PEP polymer in deuterated decane for three polymer concentrations. The solid curves show the calculated $S_p(Q)$ using Eq. (16) and the extrapolated $P_p(Q)$ in Fig. 4(b). Because hydrogenated polymer samples are used

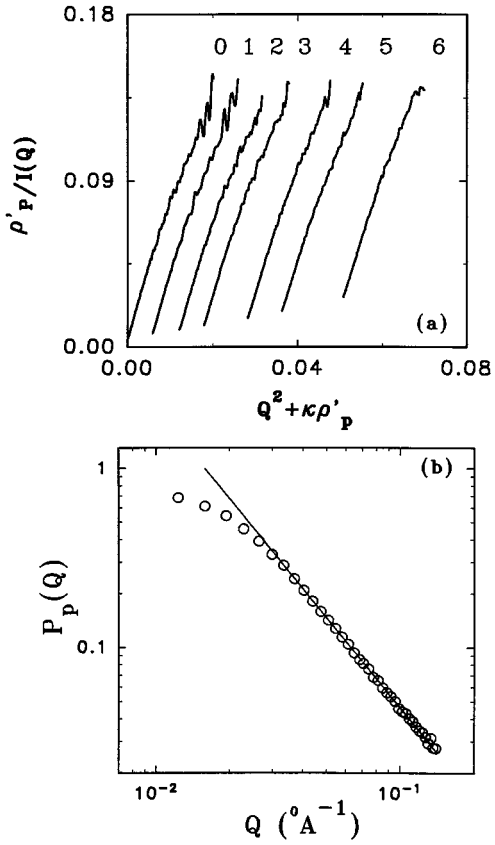

FIG. 4. (a) Zimm plot of the SANS data for the pure PEP in deuterated decane with the polymer concentration ρ_p' (g/cm^3) being (1) 0.0072, (2) 0.0151, (3) 0.0223, (4) 0.0352, (5) 0.0452, and (6) 0.0634. The zeroth curve is the extrapolated $[K_0 M_p P_p(Q)]^{-1}$ and the scale constant $\kappa=0.8$. (b) Extrapolated polymer form factor $P_p(Q)$ as a function of Q. The solid line is the fitted function $1/[0.64(QR_g)^{5/3}]$ to the circles at large Q.

in the experiment, the hydrogen atoms in the polymer sample contribute a small amount of incoherent scattering to the total intensity $I(Q)$ [which is proportional to $S_p(Q)$]. To describe the Q-independent incoherent scattering, we introduce an additive noise term τ to the calculated $S_p(Q)$ in Eq. (16). The fitted values of A_2M_p and τ are listed in Table IV. It is seen from Table IV that the contribution of the incoherent scattering to the total intensity is at a few percent level. This is consistent with our calculation of the incoherent scattering intensity for the PEP using the known incoherent cross section of the hydrogen atoms. The fitted values of A_2M_p are very close to that obtained from the Zimm analysis and they do not change very much in our working range of the polymer concentration. Figure 5 thus demonstrates that Eqs. (13) and (16) can indeed be used to describe the scattering data from the concentrated polymer samples. The measured $S_p(Q)$ in Fig. 5 shows a typical correlation hole for the polymer chains [43] and is very different from the structure factor of either a hard-sphere system (see Fig. 3) or an ideal gas (polymer at Θ point). These two models have been widely used to describe the polymer molecules in the colloidal suspension [2,22].

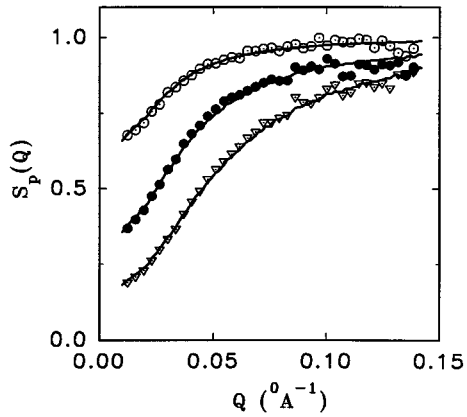

FIG. 5. Measured structure factor $S_p(Q)$ for the PEP polymer in deuterated decane. The polymer concentrations are ρ_p' (g/cm^3)=0.0072 (open circles), 0.0276 (closed circles), and 0.0634 (open triangles). The solid curves are the calculated $S_p(Q)$ using Eq. (16) and the extrapolated $P_p(Q)$ in Fig. 4(b).

TABLE IV. Fitting results from concentrated polymer samples.

ρ_p' (g/cm^3)	A_2M_p (cm^3/g)	τ
0.0038	45.0	0.02
0.0072	47.5	0.005
0.0151	41.0	0.02
0.0223	40.8	0.03
0.0276	43.0	0
0.0352	41.5	0.04
0.0452	42.0	0.05
0.0634	47.0	0.04

C. Mixtures of colloids and polymers

We now discuss the SANS data from the colloid-PEP-decane mixtures. Some of the results in this section have been briefly reported in Ref. [44]. Because decane and the PEP are both protonated, the polymer chains in the mixture are invisible to neutrons. To reduce the fitting ambiguity and pinpoint the control parameters for the depletion effect, we prepared three series of mixture samples with $\rho_c'=26.2$, 17.5, and 8.7 wt. %, respectively. For each series of the samples, ρ_c' was kept the same and the polymer concentration ρ_p' was increased until the mixture became phase separated (except for the series with $\rho_c'=8.7$ wt. %) with a visible interface, which separates the dark-brown colloid-rich lower phase from the light-brown colloid-poor upper phase. In this way all the colloidal parameters remain unchanged and one can clearly see the effect of adding polymer to the colloidal suspensions. Our previous light-scattering measurements [23] have revealed that the PEP chains do not adsorb onto the colloidal surfaces and the phase separation in the colloid-PEP mixture samples occurs at the concentrations very close to the depletion prediction.

Figure 6 compares the measured $S_c(Q)$ for three values of ρ_p' when (a) $\rho_c'=26.2$ wt. %, (b) $\rho_c'=17.5$ wt. %, and (c) $\rho_c'=8.7$ wt. %. It is seen that the main effect of adding PEP is to increase the value of $S_c(Q)$ in the small-Q region, whereas the large-Q behavior of $S_c(Q)$ remains nearly unchanged. As the colloid concentration increases, the effect of adding PEP becomes more and more pronounced. Since

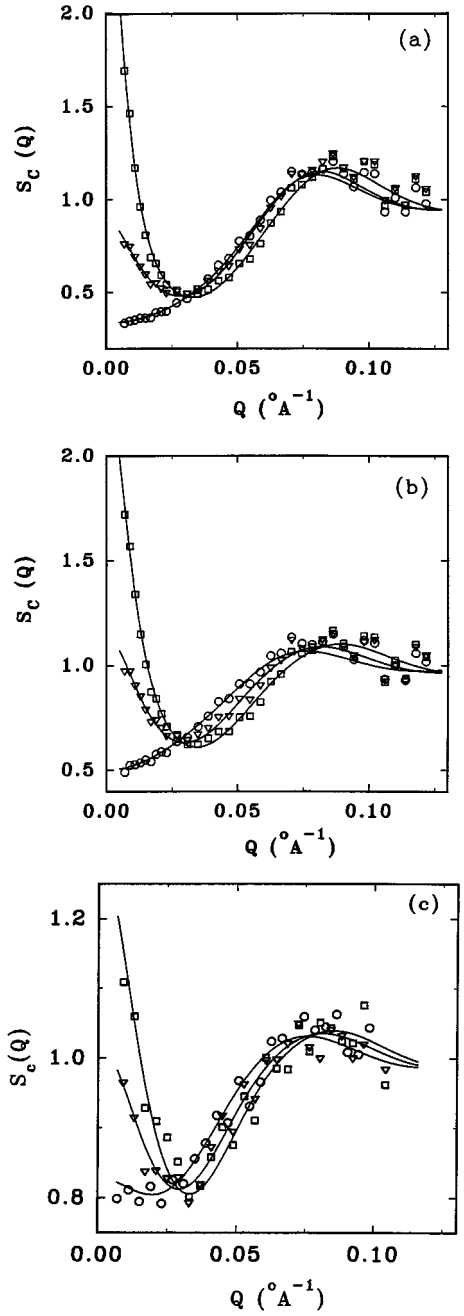

FIG. 6. Measured colloidal structure factor $S_c(Q)$ of the colloid-PEP mixtures for different polymer concentration ρ_p' when (a) $\rho_c'=26.2$ wt. %, (b) $\rho_c'=17.5$ wt. %, and (c) $\rho_c'=8.7$ wt. %. The values of ρ_p' (g/cm^3) in (a) are 0.0039 (○), 0.0165 (▽), and 0.0308 (□); those in (b) are 0.0038 (○), 0.0233 (▽), and 0.0652 (□); and those in (c) are 0.0081 (○), 0.0226 (▽), and 0.048 (□). The solid curves are the fits to Eq. (12) using the potential $U(r)$ in Eq. (9).

$S_c(0)$ is proportional to the isothermal (osmotic) compressibility of the colloidal solution, an increasing $S_c(0)$ with ρ_p' indicates an increase in the attraction between the colloidal particles. Figure 6 thus reveals a notable feature for the polymer-induced depletion attraction between the colloidal particles. The solid curves in Fig. 6 are the fits to Eq. (12) using the potential $U(r)$ in Eq. (9). There are four parameters in the fitting: The volume fraction ϕ_c and the diameter σ are for the hard-core potential; and the interaction amplitude $\tilde{P}$ and the range parameter λ describe the attraction tail. The fitting results are summarized in Table V.

TABLE V. Fitting results from three series of the colloid-PEP mixtures with three different colloid concentrations: (a) $\rho_c'=26.2$ wt. %, (b) $\rho_c'=17.5$ wt. %, and (c) $\rho_c'=8.7$ wt. %.

Sample	ρ_p' (g/cm^3)	ϕ_c	σ (nm)	$\tilde{P}$	λ
		(a)			
1	0.0	0.146	7.80	−0.1	2.9
2	0.004	0.136	7.45	−0.01	2.9
3	0.009	0.130	7.45	0.095	2.9
4	0.017	0.123	7.30	0.175	2.9
5	0.024	0.123	6.90	0.228	2.9
6	0.031	0.123	6.80	0.265	2.9
		(b)			
1	0.0	0.086	7.70	−0.06	2.9
2	0.004	0.081	7.70	−0.019	2.9
3	0.009	0.081	7.70	0.066	2.9
4	0.016	0.080	7.55	0.143	2.9
5	0.023	0.080	7.20	0.180	2.9
6	0.030	0.080	7.10	0.214	2.9
7	0.049	0.083	6.65	0.260	2.9
8	0.065	0.080	6.85	0.250	2.9
		(c)			
1	0.0	0.038	7.70	−0.033	2.9
2	0.004	0.038	7.70	−0.007	2.9
3	0.008	0.038	7.70	0.054	2.9
4	0.016	0.038	7.50	0.110	2.9
5	0.023	0.038	7.20	0.141	2.9
6	0.029	0.038	7.10	0.172	2.9
7	0.037	0.038	6.90	0.200	2.9
8	0.048	0.038	6.90	0.220	2.9

It is seen from Table V that for a fixed colloid concentration, the fitted values of σ and ϕ_c do not change very much with the polymer concentration and they are close to those obtained from the corresponding pure colloidal suspensions ($\rho_p'=0$). Furthermore, the fitted λ also remains constant for different ρ_c' and ρ_p' and its best fit value is $\lambda=2.9$. This value is close to the calculated $\lambda=1+R_g/(R_0+\delta)=3.07$. In the literature, R_g is commonly used as the effective colloid-polymer interaction range [18] and we have adopted the same convention in Eq. (9). Because polymer chains are penetrable, we expect that the actual colloid-polymer interaction range is in between the radius of gyration R_g and the thermodynamic radius R_T, which measures the polymer-polymer interaction range. From the fitted value of λ, we find the effective colloid-polymer interaction range to be 7.6 nm, which is about 10% smaller than R_g but 60% larger than R_T. To the authors' knowledge, this is the first time that a microscopic measurement is performed to provide quantitative information about the interaction range of the depletion attraction. With the above three fitting parameters fixed, we were able to fit all the scattering data from different mixture samples (19 samples in total) with only one free parameter: the interaction amplitude $\tilde{P}$.

It should be pointed out that in the above data analysis, we have assumed that the colloidal particles are identical and

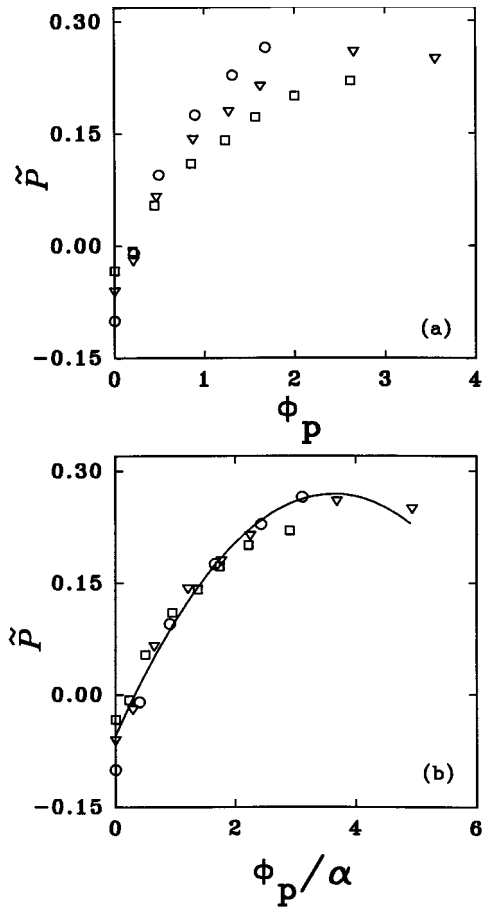

FIG. 7. Fitted interaction amplitude $\widetilde{P}$ as a function of (a) the effective polymer volume fraction $\phi_p=\rho_p'/\rho^*$ and (b) the scaled polymer volume fraction ϕ_p/α. The colloid concentrations of the mixture samples are $\rho_c'=26.2$ wt. % (○), $\rho_c'=17.5$ wt. % (▽), and $\rho_c'=8.7$ wt. % (□). The solid curve in (b) is the fitted function $\widetilde{P}=-0.054+0.178(\phi_p/\alpha)-0.0245(\phi_p/\alpha)^2$.

have considered only the polymer-induced depletion interaction between the colloidal particles. In principle, the polydispersity in particle size and a small amount of surfactant aggregates in the mixture could also introduce depletion attractions, which may cause some degree of fractionation or association in the pure colloidal suspension [11,45]. However, because the size difference between the colloidal particles is small and the polymer chains are much larger than the surfactant aggregates, the depletion effect due to the surfactant aggregates and the polydispersity in particle size should be very weak compared to the polymer-induced depletion effect and therefore it is not likely to affect our data analysis. This argument is further supported by the following facts. (i) We did not observe any substantial amount of attraction in the measured $S_c(Q)$ for the pure colloidal samples. As shown in Fig. 3, the measured $S_c(Q)$ of the pure colloidal suspensions can be well described by a hard-core potential with a weak repulsive tail. (ii) Because the colloidal parameters are the same for each series of the mixture samples with same ϕ_c, the effect seen in Fig. 6 is solely due to the addition of PEP into the colloidal suspension. (iii) Furthermore, the main effect of the small polydispersity in particle size is to average out the oscillations of $S_c(Q)$ in the large-Q range beyond the first peak position, whereas the effect of adding polymer, as shown in Fig. 6, is to increase the value of $S_c(Q)$ in the small-Q range.

Figure 7(a) shows the fitted $\widetilde{P}$ as a function of the effective polymer volume fraction $\phi_p=\rho_p'/\rho^*$, where $\rho^*=M_p/[(4\pi/3)R_g^3]$ is the polymer overlap concentration. It is seen that $\widetilde{P}$ first increases linearly with ϕ_p up to $\phi_p\simeq 1$ and then it levels off. For a given ϕ_p, $\widetilde{P}$ also depends upon ρ_c'. If the polymer molecules in the mixture are treated as an ideal gas, their osmotic pressure $\Pi_p=n_pk_BT$ and hence $\widetilde{P}=\Pi_p v_p/(k_BT)=\phi_p$. Recently, Lekkerkerker *et al.* [4,18] have pointed out that the polymer number density n_p should be defined as $n_p=N_p/V_f$, where N_p is the total number of the polymer molecules in the mixture and $V_f=\alpha(\phi_c)V$ is the free volume not occupied by the colloidal particles and their surrounding depletion zones. The free volume V_f is proportional to the sample volume V and the proportionality constant $\alpha(\phi_c)$ ($\leqslant 1$) has the form [4]

$$\alpha(\phi_c)=(1-\phi_c)e^{-(A\gamma+B\gamma^2+C\gamma^3)}, \tag{18}$$

where $\gamma=\phi_c/(1-\phi_c)$, $A=3\xi+3\xi^2+\xi^3$, $B=9\xi^2/2+3\xi^3$, and $C=3\xi^3$. In the above, $\xi=2R_g/\sigma$ is the size ratio of the polymer chain to the colloidal particle. At low ϕ_c, we have $\alpha(\phi_c)=1-\phi_c(1+\xi)^3$, where $\phi_c(1+\xi)^3$ is the volume fraction occupied by the colloidal particles and their surrounding depletion zones. It should be mentioned that Eq. (18) holds only when $\xi\leqslant 1$. For our mixture samples, however, the polymer chains are larger than the colloidal particles. In this case, Eq. (18) overestimates the volume fraction of the depletion zones and the resulting $\alpha(\phi_c)$ becomes underestimated. For example, when $\phi_c=0.14$ and $\xi=\frac{8.28}{4.0}=2.07$, we have $\alpha(\phi_c)\simeq 1-\phi_c(1+\xi)^3=-3.05$. Clearly, this is an unphysical value for $\alpha(\phi_c)$. Gast, Hall, and Russel [3] have shown that this failure in getting the correct volume for the overlapping depletion zones results from the many-body effect on the mutual overlap of the excluded shells of three or more colloidal particles. In analyzing the fitting results for $\widetilde{P}$, we find that if $\sigma/(2R_g)$, instead of $2R_g/\sigma$, is defined as the size ratio ξ, Eq. (18) can still be used to calculate $\alpha(\phi_c)$. As shown in Fig. 7(b), once ϕ_p is scaled by the calculated $\alpha(\phi_c)$ using Eq. (18) with $\xi=\sigma/(2R_g)$, the three curves in Fig. 7(a) collapse into a single master curve. The solid curve in Fig. 7(b) is the fitted function $\widetilde{P}=-0.054+0.178(\phi_p/\alpha)-0.0245(\phi_p/\alpha)^2$.

The fitted $\widetilde{P}$ consists of three terms. The small negative intercept indicates that there is a weak repulsive interaction between the soft surfactant shells of the colloidal particles (see the discussion in Sec. IV A). To have a meaningful comparison with the fitted $\widetilde{P}$ for the mixture samples, here we have used the same $U(r)$ as in Eq. (9), but changed the sign of $U(r)$ for $r>\sigma$ to fit the measured $S_c(Q)$ of the pure colloidal samples. The three data points at $\phi_p=0$ in Fig. 7(a) were obtained using the potential $U(r)$ in Eq. (9) with $\lambda=2.9$. The linear coefficient of $\widetilde{P}$ should be unity for noninteracting polymer chains (an ideal gas), but our fitted value is 0.178. One plausible reason for the deviation is that with the effective potential approach, the polymer molecules are assumed to be smaller than the colloidal particles and their number density should be much higher than that of the colloidal particles. In our experiment, however, these two assumptions are not strictly satisfied and thereby the overlap

volume $V_0(r)$ in Eq. (10) is overestimated. As a result, the fitted $\tilde{P}$ is smaller than its actual magnitude because $U(r)$ in Eq. (9) is proportional to the product of $V_0(r)$ and $\tilde{P}$. Another possibility is that in calculating $\phi_p = \rho_p'/\rho^*$, a characteristic length smaller than R_g should be used for the polymer chains. For example, if the thermodynamic radius R_T is used to estimate ϕ_p, the linear coefficient will be increased by a factor of $(R_g/R_T)^3 = (8.28/4.85)^3 \simeq 5$.

The polymer-polymer interaction, which gives rise to the quadratic term in the fitted $\tilde{P}$, can have two competing effects on the depletion attraction. It may either increase $\tilde{P}$ because the osmotic pressure of the bulk polymer solution is increased or reduce the depletion attraction because the osmotic pressure inside the narrow gap between two colloidal particles is substantially increased when the distance of the two colloidal surfaces becomes large enough such that a monolayer of polymer molecules can stay in the gap [46]. Figure 7(b) clearly shows that the polymer-polymer interaction tends to reduce the depletion attraction. Recent theoretical calculations [46–48] of the depletion attraction between two parallel plates immersed in an interacting polymer (or particle) solution have shown that the enhanced osmotic pressure within the gap between the two colloidal particles can overcome the osmotic pressure increase in the bulk polymer solution and thus produce a repulsive barrier in addition to the usual attractive well shown in Eq. (9). In these calculations, the effective colloid-polymer interaction range is assumed to be a constant (say, R_g) independent of the polymer concentration. As a result, the calculations are applicable only to the binary hard-sphere systems, in which the depletants are rigid spheres [46]. For flexible polymer chains in the semidilute regime ($\phi_p > 1$), the polymer chain-chain interactions are screened over a distance of the order of the correlation length (or mesh size) $\xi_b \simeq R_g \phi_p^{-3/4}$, which decreases with increasing polymer concentration [43]. In this regime, the self-consistent mean-field calculation by Joanny, Leibler, and de Gennes [49] indicates that the polymer segments are depleted from a shell of thickness ξ_b around each colloidal particle. The fact that the depletion layer thickness ξ_b shrinks with increasing ϕ_p in the semidilute regime can be used to explain the leveling-off effect of the fitted $\tilde{P}$ in Fig. 7(b). We note from Fig. 7(b) that at the highest polymer concentration $\phi_p \simeq 4$, the fitted $\tilde{P}$ even starts to decrease. Clearly, if this trend for $\tilde{P}$ continues, the colloid-polymer mixtures can be restabilized at higher polymer concentrations. Gast and coworkers [50,51] have used the shrinking effect of ξ_b to predict the equilibrium restabilization of electrically and sterically stabilized colloidal particles in free polymer solutions. Further experimental and theoretical studies are needed in order to have a quantitative comparison for the polymer-induced depletion potential $U(r)$ in the semidilute regime.

V. CONCLUSION

Small-angle neutron- and x-ray-scattering techniques have been used to study the depletion interaction in a mixture of a hard-sphere-like colloid and a nonadsorbing polymer. The colloidal particles used in the study were sterically stabilized $CaCO_3$ nanoparticles, the polymer used was hydrogenated polyisoprene, and the solvent was decane. By matching the scattering length density of the solvent with that of the polymer, we measured the (partial) colloidal structure factor $S_c(Q)$ of the mixture samples as well as the form and the structure factors of the pure colloidal suspension and the pure polymer solution. Under the mean spherical approximation, we calculated $S_c(Q)$ using an effective interaction potential $U(r)$ for the polymer-induced depletion attraction between the colloidal particles. It is found that the measured $S_c(Q)$ for different colloid and polymer concentrations can be well described by the depletion potential $U(r)$. The fitted amplitude $\tilde{P}$ of the depletion attraction is found to increase linearly with the polymer volume fraction ϕ_p up to $\phi_p \simeq 1$. At higher volume fractions, the polymer-polymer interaction becomes important and results in a gradual reduction in the depletion attraction. The experiment reveals that the interaction amplitude $\tilde{P}$ becomes independent of the colloid concentration, once the free volume not occupied by the colloidal particles and their surrounding depletion zones is used to calculate ϕ_p. The experiment also shows that the interaction range for the depletion attraction is about 10% smaller than the radius of gyration R_g of the polymer chains. Because the polymer molecules can be used to continuously change the range and the amplitude of the depletion interaction, our experiment depicts the effectiveness of using polymer to study interaction-related phenomena in colloidal suspensions.

ACKNOWLEDGMENTS

We have benefited from useful discussions with T. A. Witten, B. J. Ackerson, J. H. H. Perk, W. B. Russel, and J. B. Hayter. We thank D. Schneider for his assistance with the SANS measurements at the Brookhaven National Laboratory. We also acknowledge the Brookhaven National Laboratory, the National Institute of Standards and Technology, and the Oak Ridge National Laboratory for granting neutron and x-ray beam times. This work was supported by the National Aeronautics and Space Administration under Grants Nos. NAG3-1613 and NAG3-1852.

APPENDIX

The Fourier transform of the direct correlation function $C(r)$ is

$$C(Q) = \int_0^\sigma C_{\rm HS}(r) e^{-i\mathbf{Q}\cdot\mathbf{r}} d\mathbf{r} + \int_\sigma^\infty [-U(r)/(k_B T)] e^{-i\mathbf{Q}\cdot\mathbf{r}} d\mathbf{r}$$
$$= C_{\rm HS}(Q) + C_{\rm dep}(Q). \quad \text{(A1)}$$

In the above, $U(r)$ is the interaction potential given by Eq. (9) and

$$C_{\rm HS}(r) = -\alpha - \beta r - \tfrac{1}{2}\phi_c \alpha r^3 \quad \text{(A2)}$$

is the direct correlation function for a hard-sphere system [31,32]. The coefficients α and β in Eq. (A2) are given by [31,32]

$$\alpha = \frac{(1+2\phi_c)^2 + \phi_c^3(\phi_c - 4)}{(1-\phi_c)^4}, \quad \text{(A3)}$$

$$\beta = -\phi_c \frac{18 + 20\phi_c - 12\phi_c^2 + \phi_c^4}{3(1-\phi_c)^4}, \quad \text{(A4)}$$

where $\phi_c = \pi\rho_c\sigma^3/6$ is the volume fraction of the colloidal particles. The final results for $C(Q)$ in Eq. (A1) are

$$\rho_c C_{\mathrm{HS}}(Q) = -\frac{24\phi_c}{(Q\sigma)^6}\{\alpha(Q\sigma)^3[\sin(Q\sigma) - Q\sigma\cos(Q\sigma)] + \beta(Q\sigma)^2[2Q\sigma\sin(Q\sigma) - (Q^2\sigma^2 - 2)\times\cos(Q\sigma) - 2] + \tfrac{1}{2}\phi_c\alpha[(4Q^3\sigma^3 - 24Q\sigma)\times\sin(Q\sigma) - (Q^4\sigma^4 - 12Q^2\sigma^2 + 24)\times\cos(Q\sigma) + 24]\}, \tag{A5}$$

$$\rho_c C_{\mathrm{dep}}(Q) = \frac{24\phi_c}{(Q\sigma)^6}\frac{\tilde{P}}{(\lambda-1)^3}\left\{(3\lambda^2Q^2\sigma^2 - 12)\cos(\lambda Q\sigma) - 12\lambda Q\sigma\sin(\lambda Q\sigma) + \left[\lambda^4Q^4\sigma^4\left(\frac{1}{\lambda} - \frac{3}{2\lambda^2} + \frac{1}{2\lambda^4}\right) + \lambda^2Q^2\sigma^2\left(3 - \frac{6}{\lambda^2}\right) + 12\right]\cos(Q\sigma) + \left[12Q\sigma - \lambda^3Q^3\sigma^3\left(1 - \frac{3}{\lambda} + \frac{2}{\lambda^3}\right)\right]\sin(Q\sigma)\right\}. \tag{A6}$$

[1] S. Asakura and F. Oosawa, J. Chem. Phys. **22**, 1255 (1954).
[2] A. Vrij, Pure Appl. Chem. **48**, 471 (1976).
[3] A. P. Gast, C. K. Hall, and W. B. Russel, J. Colloid Interface Sci. **96**, 251 (1983).
[4] H. N. W. Lekkerkerker *et al.*, Europhys. Lett. **20**, 559 (1992).
[5] D. H. Napper, *Polymeric Stabilization of Colloidal Dispersions* (Academic, New York, 1983).
[6] B. L. Carvalho *et al.*, Macromolecules **26**, 4632 (1993).
[7] T. Biben and J.-P. Hansen, Phys. Rev. Lett. **66**, 2215 (1991).
[8] D. Frenkel and A. A. Louis, Phys. Rev. Lett. **68**, 3363 (1992).
[9] M. Dijkstra and D. Frenkel, Phys. Rev. Lett. **72**, 298 (1994).
[10] Y. Rosenfeld, Phys. Rev. Lett. **72**, 3831 (1994).
[11] J. Bibette, D. Roux, and F. Nallet, Phys. Rev. Lett. **65**, 2470 (1990).
[12] S. Sanyal, N. Easwar, S. Ramaswamy, and A. K. Sood, Europhys. Lett. **18**, 107 (1992).
[13] J. S. van Duijneveldt, A. W. Heinen, and H. N. W. Lekkerkerker, Europhys. Lett. **21**, 369 (1993).
[14] P. Kaplan, J. L. Rouke, A. G. Yodh, and D. J. Pine, Phys. Rev. Lett. **72**, 582 (1994).
[15] A. Imhof and J. K. G. Dhont, Phys. Rev. Lett. **75**, 1662 (1995).
[16] R. Piazza and G. D. Pietro, Europhys. Lett. **28**, 445 (1994).
[17] U. Steiner, A. Meller, and J. Stavans, Phys. Rev. Lett. **74**, 7450 (1995).
[18] S. M. Ilett, A. Orrock, W. Poon, and P. Pusey, Phys. Rev. E **51**, 1344 (1995).
[19] W. B. Russel, D. A. Saville, and W. R. Schowalter, *Colloidal Dispersions* (Cambridge University Press, Cambridge, 1989).
[20] *Colloid-Polymer Interactions*, ACS Symposium Series 532, edited by P. Dubin and P. Tong (American Chemical Society, Washington, DC, 1993).
[21] B. Vincent, P. F. Luckham, and F. A. Waite, J. Colloid Interface Sci. **73**, 508 (1980).
[22] H. D. Hek and A. Vrij, J. Colloid Interface Sci. **84**, 409 (1981).
[23] P. Tong, T. A. Witten, J. S. Huang, and L. J. Fetters, J. Phys. (Paris) **51**, 2813 (1990).
[24] M. Nierlich, F. Boue, A. Lapp, and R. Oberthur, Colloid Polym. Sci. **263**, 955 (1985).
[25] I. Markovic *et al.*, Colloid Polym. Sci. **262**, 648 (1984).
[26] I. Markovic and R. H. Ottewill, Colloid Polym. Sci. **264**, 65 (1986).
[27] T. P. O'Sullivan and M. E. Vickers, J. Appl. Cryst. **24**, 732 (1991).
[28] M. Kotlarchyk, S.-H. Chen, J. S. Huang, and M. W. Kim, Phys. Rev. A **29**, 2054 (1984).
[29] X.-L. Wu, P. Tong, and J. S. Huang, J. Colloid Interface Sci. **148**, 104 (1992).
[30] J.-P. Hansen and I. R. McDonald, *Theory of Simple Liquids*, 2nd ed. (Academic, London, 1991).
[31] M. Wertheim, Phys. Rev. Lett. **8**, 321 (1963).
[32] E. Thiele, J. Chem. Phys. **38**, 1959 (1963).
[33] B. H. Zimm, J. Chem. Phys. **14**, 164 (1946).
[34] B. H. Zimm, J. Chem. Phys. **16**, 1093 (1948).
[35] H. Benoit and M. Benmouna, Polymer **25**, 1059 (1984).
[36] B. Hammouda, Adv. Polym. Sci. **106**, 87 (1993).
[37] J. Mays, N. Hadjichristidis, and L. J. Fetters, Macromolecules **17**, 2723 (1984).
[38] J. Mays and L. J. Fetters, Macromolecules **22**, 921 (1989).
[39] N. S. Davidson *et al.*, Macromolecules **20**, 2614 (1987).
[40] N. W. Ashcroft and J. Lekner, Phys. Rev. **154**, 83 (1966).
[41] R. V. Sharma and K. C. Sharma, Phys. Lett. **56A**, 107 (1976).
[42] R. V. Sharma and K. C. Sharma, Physica A **89**, 213 (1977).
[43] P.-G. de Gennes, *Scaling Concepts in Polymer Physics* (Cornell University Press, Ithaca, 1979).
[44] X. Ye, T. Narayanan, P. Tong, and J. Huang, Phys. Rev. Lett. **76**, 4640 (1996).
[45] J. Bibette, J. Colloid Interface Sci. **147**, 474 (1991).
[46] Y. Mao, M. E. Gates, and H. N. W. Lekkerkerker, Physica A **222**, 10 (1995).
[47] P. B. Warren, S. M. Ilett, and W. C. K. Poon, Phys. Rev. E **52**, 5205 (1995).
[48] J. Y. Walz and A. Sharma, J. Colloid Interface Sci. **168**, 485 (1994).
[49] J. F. Joanny, L. Leibler, and P.-G de Gennes, J. Polym. Sci. Polym. Phys. Ed. **17**, 1073 (1979).
[50] A. P. Gast, C. K. Hall, and W. B. Russel, Faraday Discuss. Chem. Soc. **76**, 189 (1983).
[51] A. P. Gast and L. Leibler, Macromolecules **19**, 686 (1986).